JKAS
Journal of the Korean Astronomical Society
http://jkas.kas.org
eISSN: 2288-890X · pISSN: 1225-4614
JKAS (2023), **56**, 2, 159–168
doi: 10.5303/JKAS.2023.56.2.159

KVNCS: 2. The Fringe Survey of New Candidates for VLBI Calibrators in the K Band

Jeong Ae Lee[1,⋆], **Taehyun Jung**[1,2], **Bong Won Sohn**[1,2], **and Do-Young Byun**[1,2]

[1]Korean Astronomy and Space Science Institute, 776, Daedeokdae-ro, Yuseong-gu, Daejeon, Republic of Korea
[2]University of Science ans Technology, Yuseong-gu, Daejeon, Republic of Korea
⋆Corresponding Author: J. A. Lee, jalee@kasi.re.kr

Received May 14, 2023; Accepted July 4, 2023; Published July 31, 2023

Abstract

The main goal of the Korean VLBI Network Calibrator Survey (KVNCS) is to expand the VLBI calibrators catalog for KVN, KaVA (KVN and VERA Array), EAVN (East-Asian VLBI Network), and other extended regions. The second KVNCS (KVNCS2) aimed to detect VLBI fringes of new candidates for calibrators in the K band. Out of the 1533 sources whose single-dish flux density in the K band was measured with KVN telescopes (Lee et al. 2017), 556 sources were observed with KVN in the K band. KVNCS2 confirmed the detection of VLBI fringes of 424 calibrator candidates over a single baseline. All detected sources had a high Signal-to-Noise Ratio (SNR) of >25. Finally, KVNCS2 confirmed 347 new candidates as VLBI calibrators in the K band, resulting in a 5% increase in the sky coverage compared to previous studies. The spatial distribution was quasi-uniform across the observable region (Dec. > −32.5°). In addition, the possibility as calibrator candidates for the detected sources was checked, using an analysis of the flux-flux relationship. Ultimately, the KVNCS catalog will not only become the VLBI calibrator list but is also useful as a database of compact radio sources for astronomical studies.

Keywords: catalogues — surveys — astrometry — galaxies: active — radio continuum: galaxies — quasars: general

1. Introduction

The Korean VLBI Network Calibrator Survey (KVNCS) aims to secure high-frequency (>20 GHz) Very Long Baseline Interferometer (VLBI) calibrators for KVN and other high-frequency VLBI systems. A dense distribution of calibrators in the sky is essential to apply phase referencing (PR) techniques. VLBI calibrators have been used for conventional phase referencing in order to increase the coherence time so as to detect faint sources and to measure the accurate position of sources in VLBI astrometry (e.g., Beasley & Conway 1995; Ma et al. 1998; Fomalont et al. 2003; Petrov et al. 2005, 2006; Kovalev et al. 2007; Petrov et al. 2008; Gordon et al. 2016; Charlot et al. 2020). In case of KVN, the calibrators in the K band are crucial for the frequency phase transfer (FPT) technique enabled by the simultaneous multi-frequency (22/43/86/129 GHz) receiving system (e.g., Han et al. 2008; Lee et al. 2011, 2014; Zhao et al. 2018, 2019), because phase solutions at the lower frequencies (e.g., 22 or 43 GHz) is used to compensate atmospheric phase fluctuations at high frequencies (e.g., 43, 86 and 129 GHz) (e.g., Jung et al. 2011; Dodson et al. 2014; Rioja et al. 2015).

The VLBA Calibrator Survey (VCS, 1–6; Beasley & Conway 1995; Fomalont et al. 2003; Petrov et al. 2005, 2006; Kovalev et al. 2007; Petrov et al. 2008) is a well-defined monitoring survey aimed at searching for and increasing the number of calibrators. VCS9, the final VCS, provides the position of 5447 sources and the images of 5649 sources in the S and X bands[1]. In addition, the database of International Celestial Reference Frame (ICRF) can also be used to identify VLBI calibrator candidates[2], because VLBI calibrators show compact structures and have stable positions. Several thousand sources have been monitored over about 20 years to realize the reference frame, and the positions of 212, 295, and 303 sources are defined by ICRF1, ICRF2, and ICRF3 in the S and X bands, respectively. Additionally, the positions of 824 sources at 24 GHz and 678 at 32 GHz are supplemented in ICRF3. Recently, the structure information of 731 sources based on ICRF3 in the K band was obtained by de Witt et al. (2023). Among them, we selected 659 sources, which their structure indices are lower than 3, to compare with this study.

VLBI observation at high-frequency is useful to understand the environment of optically thick objects and to improve the astrometric accuracy with compact sources. Recently, sev-

[1]http://astrogeo.org/vcs9/
[2]https://www.iers.org/IERS/EN/Home/home_node.html

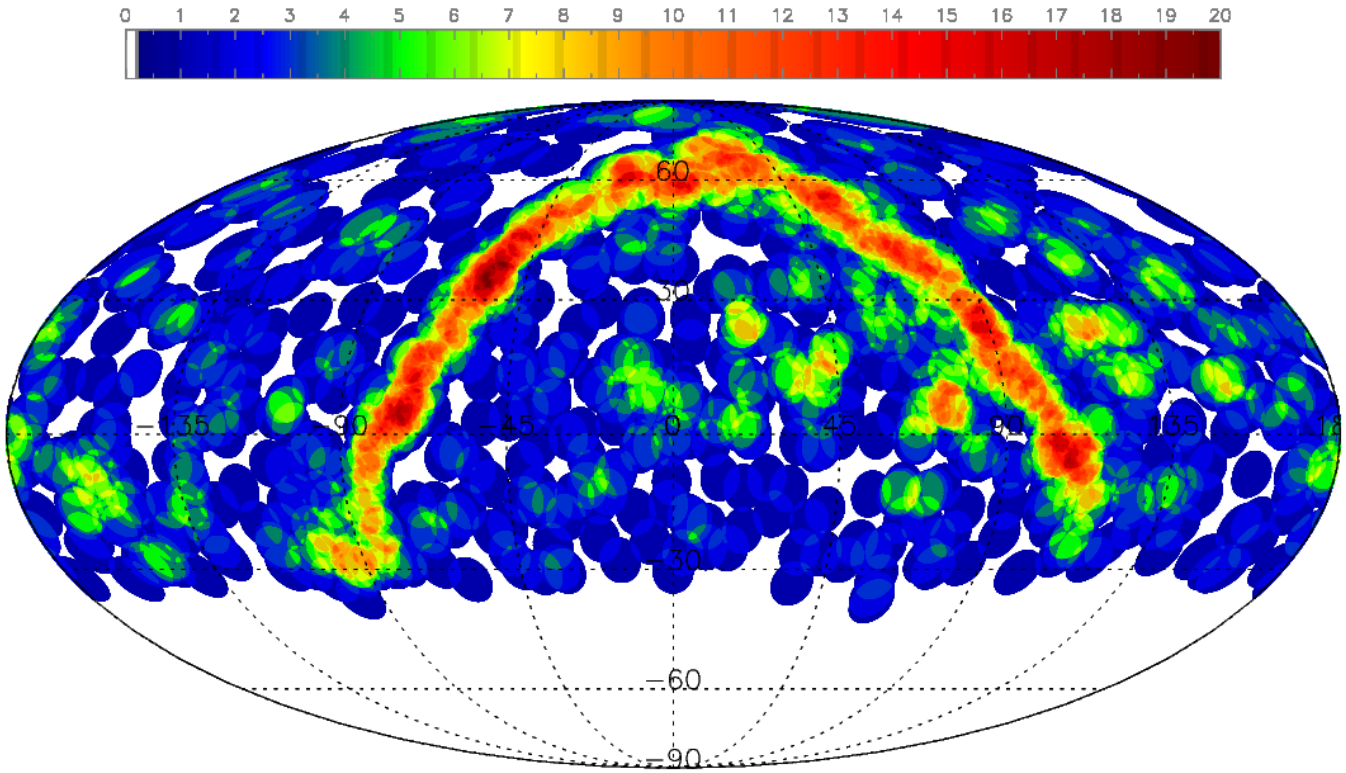

Figure 1. Spatial distribution of 1079 known K-band calibrators or candidates, named Cal-K in this study. The radius of each circle is 5°, where it is assumed each source is located in the center of each circle. The colored legend shows the values represented by overlapping circles. This map is drawn using a Mollweide equal-area projection (abscissa: right ascension [°], ordinate: declination [°]).

eral studies have detected candidates of calibrators at high-frequency, but the available calibrators are still insufficient. The reason for this is that their celestial distribution is concentrated on Galactic plane, and furthermore there are only one or two calibrators in the near the target sources. Figure 1 shows the sky coverage of 1079 sources in the K band with VLBI (Charlot et al. 2010; Petrov et al. 2011, 2012; Petrov 2012; de Witt et al. 2023). Their distribution was drawn with a 5° radius of circles, which is the separation angle between sources. We denote these studies as Cal-K in this study.

The first KVNCS (KVNCS1) provides the single-dish flux-density of 1533 and 553 sources at 22 (K band) and 43 (Q band) GHz, respectively (Lee et al. 2017). The 1533 sources cover 99% of the observable sky at KVN stations, assuming a 5° separation angle between sources, and distribute a quasi-uniformly in the sky. Dodson et al. (2014) suggests that the separation between a target and a calibrator is efficient within 5.7° for the source-frequency PR. Referring to their result, this study used a 5° separation angle for analyzing the spatial distribution. KVNCS1 serves as a database for VLBI studies and the targets of the KVN legacy project, known as Multi-frequency Active Galactic Nuclei (AGN) Survey with the KVN (MASK, Jung 2018), were selected from KVNCS1. Some studies used the flux-density of KVNCS1 sources (e.g., Krezinger et al. 2022; An et al. 2022). Thus, we performed the VLBI fringe detection survey in order to increase the possibility of KVNCS sources as candidates of VLBI calibrators, which has been named the second KVN calibrator Survey (KVNCS2), following KVNCS1. From the results, 556 targets of KVNCS2 detected in KVNCS1 are AGNs which include 385 flat-spectrum radio sources, 45 Quasi-Stellar Objects, 16 BL Lacs, 14 young AGNs, 9 Syfert galaxies, and 86 others[3], and the details of the target selection, observation, and data reduction methods are introduced in Sections 2 and 3. In Section 4, we present the results, our findings, and future prospects of KVNCS2. Finally, we summarize this study in Section 5.

2. Source Selection and Observation

Among 1533 sources that were detected in single-dish mode in the K band, 675 sources, that did not overlap with previous studies (Charlot et al. 2010; Petrov et al. 2011, 2012; Petrov 2012) at that time were selected initially. To improve the detection rate of the VLBI fringe survey, targets were selected based on a single-dish flux-density of over 200 mJy at 22.7 GHz from KVNCS1. We considered not only the KVN baseline sensitivity (σ_b) in the K band, which was around 10 mJy at that time (Lee et al. 2014), but also 30–40% missing-flux between single-dish and VLBI (Lee et al. 2017). As a result, 556 sources were chosen for the fringe survey.

The KVN-VLBI system was used for the observations from February to May in 2012, September 2013, and December 2014, denoted as KVNCS2.1, KVNCS2.2, and KVNCS2.3, respectively. Unfortunately, the KVNCS2.2 data

[3]The data of AGN activity come from NASA/IPAC EXTRAGALACTIC DATABASE (https://ned.ipac.caltech.edu/).

Table 1. Observational information

Date	Observation code	Sources [count]	Scans [count]	$Tsys^{*}_{m}$ KT[a] / KU[b] / KY[c] [K]	$\tau^{\dagger}_{0,m}$ KT / KU / KY	$SEFD^{\dagger\dagger}$ KT / KU / KY [Jy]
KVNCS2.1 (KVN)						
2012-Feb -2	k12033a	157	157	126 / 95 / 87	0.04 / 0.02 / 0.03	1703 / 1222 / 1067
2012-Apr -4	k12095a	113	114	102 / 102 / 103	0.06 / 0.05 / 0.07	1379 / 1356 / 1493
	k12095b	59	70	97 / 106 / 95	0.06 / 0.07 / 0.06	1311 / 1409 / 1377
2012-Apr -5	k12096a	220	246	87 / 90 / 86	0.05 / 0.04 / 0.05	1176 / 1196 / 1247
2012-May-22	k12143a	184	215	147 / 139 / 126	0.23 / 0.17 / 0.16	1987 / 1847 / 1827
KVNCS2.3 (KVN)						
2014-Dec-7	s14jl01a	355	766	94 / 103 / 57	0.07 / 0.05 / 0.05	1281 / 1325 / 791
2014-Dec-10	s14jl01b	74	160	87 / 93 / 58	0.05 / 0.03 / 0.03	1186 / 1196 / 804
2014-Dec-17	s14jl01c	218	476	102 / 94 / 60	0.05 / 0.03 / 0.03	1390 / 1209 / 832
2014-Dec-24	s14jl01d	363	734	95 / 99 / 61	0.05 / 0.04 / 0.03	1295 / 1273 / 846

*Median system temperature. †Median zenith optical depth. ††Averaged system equivalent flux density (SEFD). [a]KT: KVN Tamna observatory. [b]KU: KVN Ulsan observatory. [c]KY: KVN Yonsei observatory. Aperture efficiency was applied depending on each observation season (https://radio.kasi.re.kr/status_report/files/Status_Report_EAVN_2023A.pdf).

could not be used due to bad weather. The frequency was set to 21.700–22.180 GHz with 256 MHz (16×16 MHz) bandwidth, and the observed data were recorded by MK5b with 1 Gbps. The integration time for each source was 120 seconds for a single scan. Table 1 shows the detailed observational information, including the observation dates and codes, the number of observed scans and sources, the median values of system temperature, optical depth, and averaged system equivalent flux density (SEFD). The observation schedule was composed by using *Sur_sked* software,[4] and we set Astromet-13 mode of *Sur_sked*, which is optimized to observe each source with short slewing in between. In KVNCS2.1, 36 positional calibrators[5] that were defined by Leonid Petrov were observed every hour for 60 seconds, and among them, a few bright sources were used as a fringe-finder. Before the first scan, the pointing offset and focus were corrected. Sky-dipping ('SkyDip') hourly and chopper-wheel calibration ('Cal') at every scan were performed to measure the sky opacity and system temperature, respectively. Of 556 sources chosen for the fringe survey, 445 were detected over a single baseline in KVNCS2.1 and were re-observed in KVNCS2.3 to check for re-detection. Each source was observed at least twice. Twenty-one calibrators with over 500 mJy of total flux density at 24 GHz were used as the fringe-finders, and the structural calibrators were taken from Lanyi et al. (2010). The other observation settings were the same as those in KVNCS2.1.

3. Data Analysis

Data were correlated on DiFX-2 software correlator (Deller et al. 2011) in Daejeon and stored the output in FITS-IDI format (Eric Greisen, NRAO memo 114).[6] The correlated data were then processed using the Astronomical Imaging Processing System (AIPS),[7] a conventional program for analyzing VLBI data. AIPS was used to perform fringe-fitting, amplitude calibration, and imaging, providing a step-by-step solution for each process.

For the KVNCS2 project, we applied the following AIPS processing steps: 1) Set the digital correction parameter (digicor) to '1' during data loading to correct quantization loss in amplitudes measurements of cross- and auto-correlation powers in the pre-processing step. We calibrated the system temperature and receiver gain using information from the 'ANTAB' file, while ignoring ionospheric effects.
2) Performed the **FRING** task twice to carry out 'manual' and 'global' fringe-fittings, respectively, correcting for errors due to system and atmospheric factors. The solution interval ('solint') was set to two minutes, which matches the observational integration time. The signal to noise ratio (SNR) cutoff was set to 5.
3) Applied the **APCAL** task with 'TY' and 'GC' tables from 'ANTAB' file for amplitude calibration, and **BPASS** task for bandpass calibration, and
4) Estimated the averaged visibility amplitude on each baseline by channel averaging with **AVSPC** and **UVAVG**, respectively, using 51 to 450 channels and 2 to 15 IFs for the averaging, while trimming the edge channels and IFs. Finally, we applied the correction factor as described (Lee et al. 2015) to obtain the final averaged visibility amplitudes.

4. Results and Discussion

4.1. Fringe Detection

Observations of 556 sources were conducted to check their detectability, and VLBI fringes were detected for 445 sources in KVNCS2.1. To verify the repeatability of the detection, a second fringe survey (KVNCS2.3) was performed with the same 445 sources. VLBI fringes for 424 out of 445 sources were

[4] http://astrogeo.org/sur_sked/
[5] http://astrogeo.org/
[6] ftp://ftp.aoc.nrao.edu/pub/software/aips/TEXT/PUBL/AIPSMEM114.PDF
[7] http://www.aips.nrao.edu/index.shtml

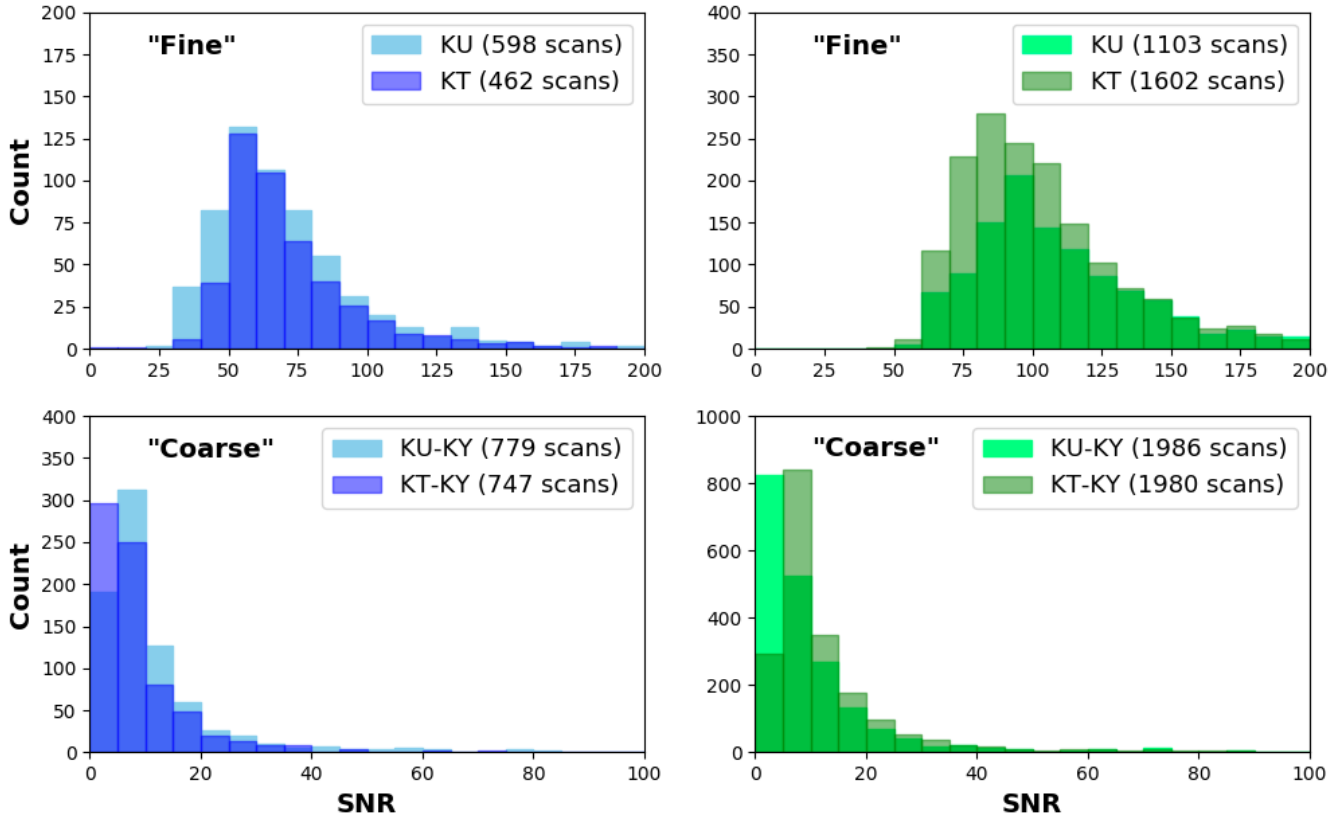

Figure 2. The histogram of signal-to-noise ratio (SNR) less than 200. The reference station is applied as KVN Yonsei (KY). Left (KVNCS2.1): Top—Station-based SNR from AIPS of 462 scans of 432 sources (KU) and 598 scans of 373 sources (KT) (SNR > 200: 12 scans of 10 sources (KU) and 14 scans of 8 sources (KT)). Bottom—Baseline-based coarse fringe-search SNR from AIPS of 779 scans of 439 sources (KU-KY) and 747 scans of 378 sources (KT-KY) (SNR > 200 : 4 scans of 3 sources (KU-KY) and 3 scans of 3 sources (KT-KY)). Right (KVNCS2.3): Top—Station-based SNR from AIPS of 1103 scans of 374 sources (KU) and 1602 scans of 389 sources (KT) (SNR > 200: 100 scans of 15 sources (KU) and 77 scans of 30 sources (KT)). Bottom—Baseline-based coarse fringe-search SNR from AIPS of 1986 scans of 385 sources (KU-KY) and 1980 scans of 415 sources (KT-KY) (SNR > 200: 11 scans of 4 sources (KU-KY) and 10 scans of 4 sources (KT-KY)).

re-checked, and the number of detected sources and the detection rate on each baseline are presented in Table 2. The VLBI fringes were detected for 76% of 556 sources in KVNCS2 in total. Although the weather conditions in KVNCS2.3 were better than those in KVNCS2.1, 21 sources were not detected. These sources were likely affected by the intrinsic brightness variation of each source.

Figure 2 shows the signal-to-noise ratio (SNR) distribution of all scans. The final SNR is obtained from AIPS's FRING task, which is defined as the SNR obtained per visibility (Desai 1998). The fringe-search procedure typically involves 1) performing baseline-based coarse fringe fitting for baselines with SNR above the cutoff; 2) searching for VLBI fringes; and 3) providing the final SNR in each station. In this study, the SNR cutoff in AIPS was set empirically at 5, and the coarse fringe fitting outputs with a SNR lower than the cutoff were not used to calculate the final fringe detection. The bottom panels show the distribution of coarse fringe search outputs. The top panels in Figure 2 present the number distribution of final SNRs, ranging from 0 to 200. For both observations, most of the detected scans have SNRs over 25. In addition, we excluded scans with an averaged visibility amplitude lower than $10\sigma_b$, based on the KVN baseline sensitivity

Table 2. The number and rate of detection

Observation (observed sources)	≥1 baseline [count]	3 baseline [count]	KT* [count]	KU† [count]
KVNCS2.1 (556 sources)	445 80.0%	376 67.6%	381 68.5%	442 79.5%
KVNCS2.3 (445 sources)	424 95.3%	375 84.3%	419 94.2%	389 87.4%

The reference antenna is the KVN Yonsei observatory (KY). *KT: KVN Tamna observatory. †KU: KVN Ulsan observatory.

(σ_b = 6.1 mJy) in the K band (*EAVN Status Report 2023A*)[8]. Finally, Table 3 presents the 424 detected sources.

Table 3 is a part of the KVNCS2 catalog. The catalog lists SNRs (columns (3)–(4)), UV distance (columns (5)–(7)), and averaged visibility amplitudes (columns (8)–(10)) of all detected scans for 424 sources. Additionally, column (12) identifies the new detection in the K band as VLBI calibrator candidates in KVNCS2. We compared the 424 detected sources with Cal-K and previous K-band astrophysical VLBI

[8] https://radio.kasi.re.kr/status_report/files/Status_Report_EAVN_2023A.pdf)

Table 3. The part of KVNCS2 Catalog

IAU name [J1950] (1)	IVS name (2)	SNR KT (3)	SNR KU (4)	KT-KU [$k\lambda$] (5)	KT-KY [$k\lambda$] (6)	KU-KY [$k\lambda$] (7)	KT-KU [Jy] (8)	KT-KY [Jy] (9)	KU-KY [Jy] (10)	Obscode (11)	New detection Y/N (12)
0006+397	0006+397	74.5	75.6	26577.391	34862.116	15448.171	0.120	0.118	0.090	s14jl01d	Y
0006+397	0006+397	79.5	78.3	26574.067	35765.393	—	0.096	0.123	—	s14jl01d	Y
0006+397	0006+397	61.5	—	—	36360.786	—	—	0.166	—	s14jl01a	Y
0006+397	0006+397	65.3	—	—	36317.744	—	—	0.173	—	s14jl01a	Y
0007+171	0007+171	—	65.5	17637.824	—	19626.098	0.145	—	0.128	s14jl01c	Y
0007+171	0007+171	93.0	93.3	21831.423	36337.822	19002.963	0.234	0.089	0.138	s14jl01d	Y
0007+171	0007+171	65.7	—	—	36391.565	—	—	0.098	—	s14jl01a	Y
0007+171	0007+171	82.5	83.7	22674.615	36411.837	15508.847	0.108	0.133	0.156	s14jl01d	Y
0007+171	0007+171	83.6	93.1	21979.729	36369.439	18845.204	0.129	0.162	0.150	s14jl01c	Y
0007+171	0007+171	87.1	—	—	35836.146	—	—	0.242	—	s14jl01a	Y

(1) IAU names [J1950], (2) IVS names, (3) SNR in KT, (4) SNR in KU, (5), (6), and (7) are UV distances, (8), (9), and (10) are the averaged visibility amplitudes, (11) is observation code in Table 1, and (12) means a Yes (Y) or No (N) of new detection in KVNCS2. The entire table is available at https://github.com/JKAS-Hub/Supp/tree/main/v56n2p159/.

studies for individual sources (Lee et al. 2016; Angioni et al. 2019; Charlot et al. 2020; Traianou 2020). As a result, we confirmed 347 new detections in the K band as VLBI calibrator candidates.

4.2. Spatial Distribution

Figure 3 presents the spatial distribution (top) and the sky coverage (bottom) of the K-band VLBI calibrator candidates. The top panel shows the spatial distribution of 424 sources detected in KVNCS2 (blue dots), 1533 sources from KVNCS1 (yellow green dots) and 1079 sources from Cal-K (blue empty circles) sources. The spatial distribution of 424 detected sources shows a quasi-uniform distribution above $-32.5°$ declination, but many Cal-K sources are concentrated on the galactic plane. The sky coverage by both the 424 detected and 1079 Cal-K sources is shown in the bottom panel of Figure 3. Coverage is improved by about 5% in the observable sky ($\geq -32.5°$), compared to Cal-K alone (see Figure 1). This plot was drawn by assuming a 5° separation angle between sources, which is the radius of circles. Colored regions, except for white, indicate an effective sky where at least one calibrator or candidate is present. Furthermore, assuming 3° and 2.2° separation angles, the covered regions of KVNCS2+Cal-K, comparing to Cal-K alone, are improved by about 9% and 7%, respectively. KVNCS2 obtains not only the improved coverage, but also a greater number of calibrator candidates. Figure 4 shows the number of overlapped regions, comparing between all K-band calibrator candidates including KVNCS2 and Cal-K except for a galactic plane region ($-5° <$ galactic latitude (b) $< 5°$). This indicates that we can find a 2–10 times greater number of calibrator candidates near the targets than those of Cal-K alone.

On the other hand, Figure 5 shows the spatial distribution on the galactic coordinate, used the Delaunay Triangulation method. In Figure 5(a), because there are large triangles at low declination ($<-32.5°$) that were not observed, these are neglected for the analysis. In order to check how close the sources are, the circumcircle radius of triangles on the sphere was calculated. Their number distribution is shown in Figure 6. The count was applied for the region in $b \leq -5°$ and $5° \geq b$ (see Figure 5(b) and (c)). Considering the circumcircle radius less than 10°, 1) KVNCS2+Cal-K : Mean and median values of circumcircle radius of triangles are 3.89° and 3.62°, respectively. 2) Cal-K alone : The mean and median values are 4.57° and 4.37°, respectively. Therefore, KVNCS2 increases the number of close calibrator candidates and improves the possibility of searching for effective calibrators.

4.3. Flux-Flux Relationship

4.3.1. KVNCS3.1: Pilot Imaging Survey

The structure information is necessary to confirm the detected sources in KVNCS2 as calibrators. For the next step, VLBI imaging studies are being conducted to obtain structural information for KVNCS sources (denoted as KVNCS3). This study uses the flux-density of KVNCS3 imaging results only to obtain the flux-flux relationship. A more detailed analysis will be presented in the near future (Lee et al., in prep.). Table 4 presents the observational information of the first KVNCS imaging survey (KVNCS3.1), which was performed using KVN and VERA Array (KaVA) with 73 sources. These selected sources have a single-dish flux density above 500 mJy and a flat spectrum in the K and Q bands from KVNCS1, and detected their VLBI fringes from KVNCS2. Observations were performed in snapshot mode with 16 IFs x 16 MHz bandwidth. The total integration time of individual sources is approximately 30 minutes and at least twice for 24 hours. The data were correlated by the Korea-Japan Correlation Center (KJCC) (Lee et al. 2015) and processed using the conventional method in AIPS. To obtain the imaging results, the data were calibrated using Difmap. The total and unresolved fluxes of the VLBI images were derived by fitting a circular-Gaussian model. The compactness of sources was calculated by the ratio of both values, and the distribution of these values is shown in Figure 7(a) (Lee 2017). Forty-nine out of 73 sources have compactness greater than or equal to 0.8.

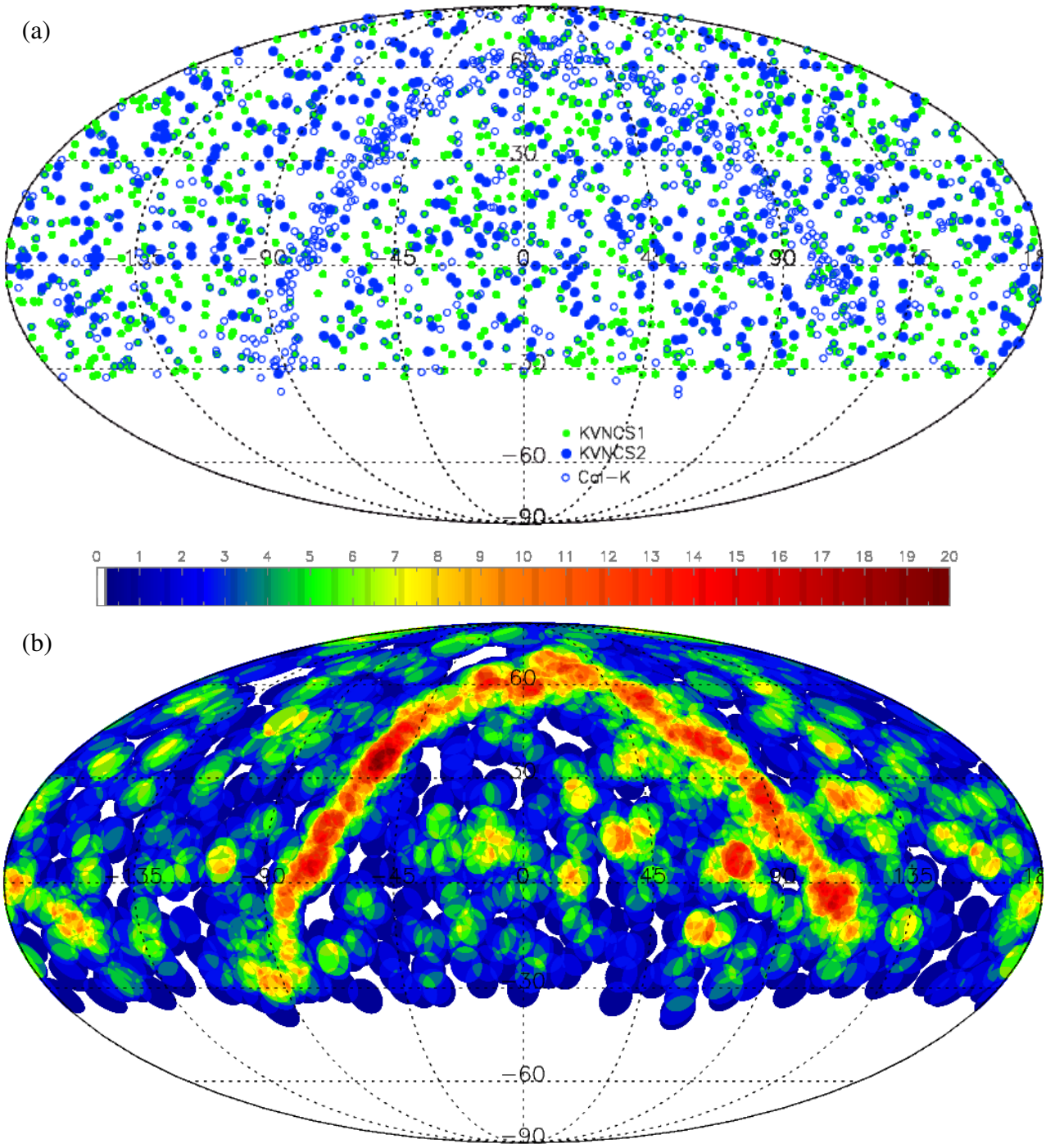

Figure 3. (a) Spatial distribution of all detections of KVNCS and Cal-K. Blue dots are 424 detected sources in KVNCS2. Yellow-green dots and blue empty circles show 1533 single-dish detected sources (KVNCS1, Lee et al. 2017) and 1079 known K-band calibrators or candidates (Cal-K, Charlot et al. 2010; Petrov et al. 2011, 2012; Petrov 2012; de Witt et al. 2023). (b) Sky coverage of 424 sources of KVNCS2 and 1079 sources of Cal-K, by assuming a 5° separation angle between sources. The colored legend shows the values represented by overlapping circles. Colored and empty regions occupy 91% and 9% of observable regions. The observation limit of source declination is −32.5°. The Mollweide equal-area projection technique was applied (abscissa: R.A. [°], ordinate : Dec. [°]).

4.3.2. Flux-Flux Relationship

To improve the possibility as calibrator candidates for the detected sources in KVNCS2, we attempted to compare the fluxes between KVNCS2 and KVNCS3.1. For simplicity, KVNCS2 and KVNCS3.1 are written as KVN and KaVA in this section. Seventy-three sources in KaVA are common sources, comparing to KVN. However, 11 out of 73 sources were detected in a single-baseline only with KVN, and 62 sources were used in this analysis. UV data of the 62 sources in KVN were extracted from AIPS, and the imaging processing was performed using Difmap. After applying phase self-calibration, the total flux was derived by fitting a circular-Gaussian model. The visibility amplitude was not modified. Table 5 shows a part

Table 4. Observational information of the first imaging survey

Date	Observation code	Sources [count]	$Tsys^{*}_{m}$ [K]	$\tau^{\dagger}_{0,m}$	SEFD†† [Jy]
			KVNCS3.1 (KaVA)		
2015-Mar-4	k15jl01a	41	150 / 152 / 263 / 336	0.12 / 0.08 / 0.20 / 0.22	2997 / 2843 / 4817 / 7205
			107 / 105 / 69	0.04 / 0.04 / 0.07	1446 / 1396 / 1000
2015-Mar-23	k15jl01b	33	151 / 125 / 124 / 414	0.08 / 0.12 / 0.12 / 0.12	3017 / 2338 / 2271 / 8877
			86 / 102 / 76	0.04 / 0.04 / 0.04	1162 / 1356 / 1102

*Median system temperature (Mizsawa/Iriki/Ogasawara/Isigaki/KT/KU/KY), †Median zenith optical depth (Mizsawa/Iriki/Ogasawara/Isigaki/KT/KU/KY), ††System equivalent flux density (SEFD, Mizsawa/Iriki/Ogasawara/Isigaki/KT/KU/KY). Aperture efficiency was applied, using 2015 season's data (https://radio.kasi.re.kr/status_report.php?cate=KaVA).

Table 5. Part of Imaging results of 62 sources from KVNCS2

IAU name [J2000] (1)	IVS name (2)	S_{total} [Jy] (3)	$S_{unresolved}$ [Jy] (4)	S_{peak} [Jy/beam] (5)	rms [Jy/beam] (6)	b_{maj} [mas] (7)	b_{min} [mas] (8)	Position Angle [°] (9)	Dynamic range (10)	Image quality (11)
J0059+0006	0056−001	0.286894	0.287	0.294	0.020	11.60	2.91	−52.7	15	0.584
J0108+0135	0106+013	2.185800	2.186	2.030	0.011	5.22	3.66	−84.6	187	0.667
J0116−1136	0113−118	0.986155	0.986	0.877	0.013	13.00	3.17	−50.7	70	0.565
J0132−1654	0130−171	0.917403	0.917	0.901	0.004	7.81	3.76	−47.4	243	0.718
J0211+1051	0208+106	1.324200	1.324	1.290	0.003	5.45	3.30	−87.5	406	0.657
J0405−1308	0403−132	1.030360	1.030	1.030	0.006	5.39	4.11	−75.8	163	0.579
J0410+7656	0403+768	0.325257	0.325	0.327	0.019	5.82	3.75	−74.2	17	0.644
J0407−1211	0405−123	1.271160	1.271	1.190	0.003	5.50	4.00	−70.3	454	0.703
J0453−2807	0451−282	2.033480	2.033	1.970	0.006	10.80	4.00	−38.4	326	0.635
J0512+4041	0509+406	1.537000	1.537	1.380	0.001	6.41	3.13	−60.3	920	0.754
J0517+4537	0513+455	0.573006	0.528	0.486	0.002	6.32	3.21	−59.5	235	0.803

(1) IAU names [J2000], (2) IVS names, (3) Total flux, (4) Unresolved flux, (5) Peak brightness, (6) Map residual, (7) Major FWHM, (8) minor FWHM, (9) Position Angle, (10) Dynamic range, and (11) Image quality factor. The entire table is available at https://github.com/JKAS-Hub/Supp/tree/main/v56n2p159/.

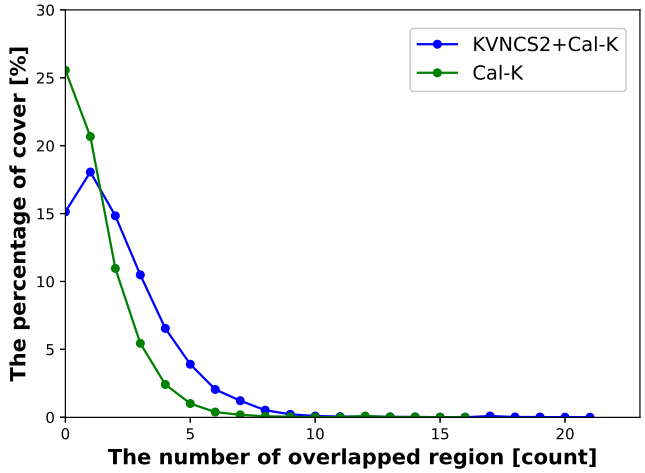

Figure 4. The percentage of coverage according to the number of overlapped regions except for a galactic plane region (−5° < galactic latitude < 5°). Blue and green lines and dots are from KVNCS2+Cal-K and Cal-K alone, respectively.

of the imaging results of the 62 sources in KVN. The total (column (3)) and unresolved (column (4)) flux-density, and peak brightness (column (5)) from the model-fitting are given. The image quality factor in column (11) is included to confirm the quality. Their distribution is provided in the top panel of Figure 7(b). The image quality factor ($S_r/S_{r,\mathrm{exp}}$) defined in Lobanov et al. (2006) was applied. S_r and $S_{r,\mathrm{exp}}$ are the measured and expected maximum amplitudes, respectively, in the residual map. $S_{r,\mathrm{exp}}$ is indicated in Equation (1). σ_r is a residual root-mean square (rms) in the residual map and N_{pix} is the number of pixels on the map. The image quality factor of KVN-VLBI observation only is generally known as 0.4–0.7 (Lee et al. 2016). The distribution of the image quality factor of KVN is well followed in the top of Figure 7(b), indicating that the KVN images traced their structure well within their limitations. The number distribution of the image quality factor of KaVA is closed to 1 in the bottom of Figure 7(b), although a few sources have large values. We can use these image results for analyzing this relationship.

$$\left|S_{r,\mathrm{exp}}\right| = \sigma_r \left[\sqrt{2}\ln\left(\frac{N_{\mathrm{pix}}}{\sqrt{2\pi}\sigma_r}\right)\right]^{1/2} \quad (1)$$

Figure 7(c) shows the flux-flux relationship between KVN and KaVA. The left panel presents the relationship between the single-dish flux density from KVNCS1 with the total fluxes derived from KVN and KaVA. In general, due to the limitation of UV coverage of VLBI data, missing-flux is about 30–40% (e.g., Lee et al. 2017) and this study obtains a similar

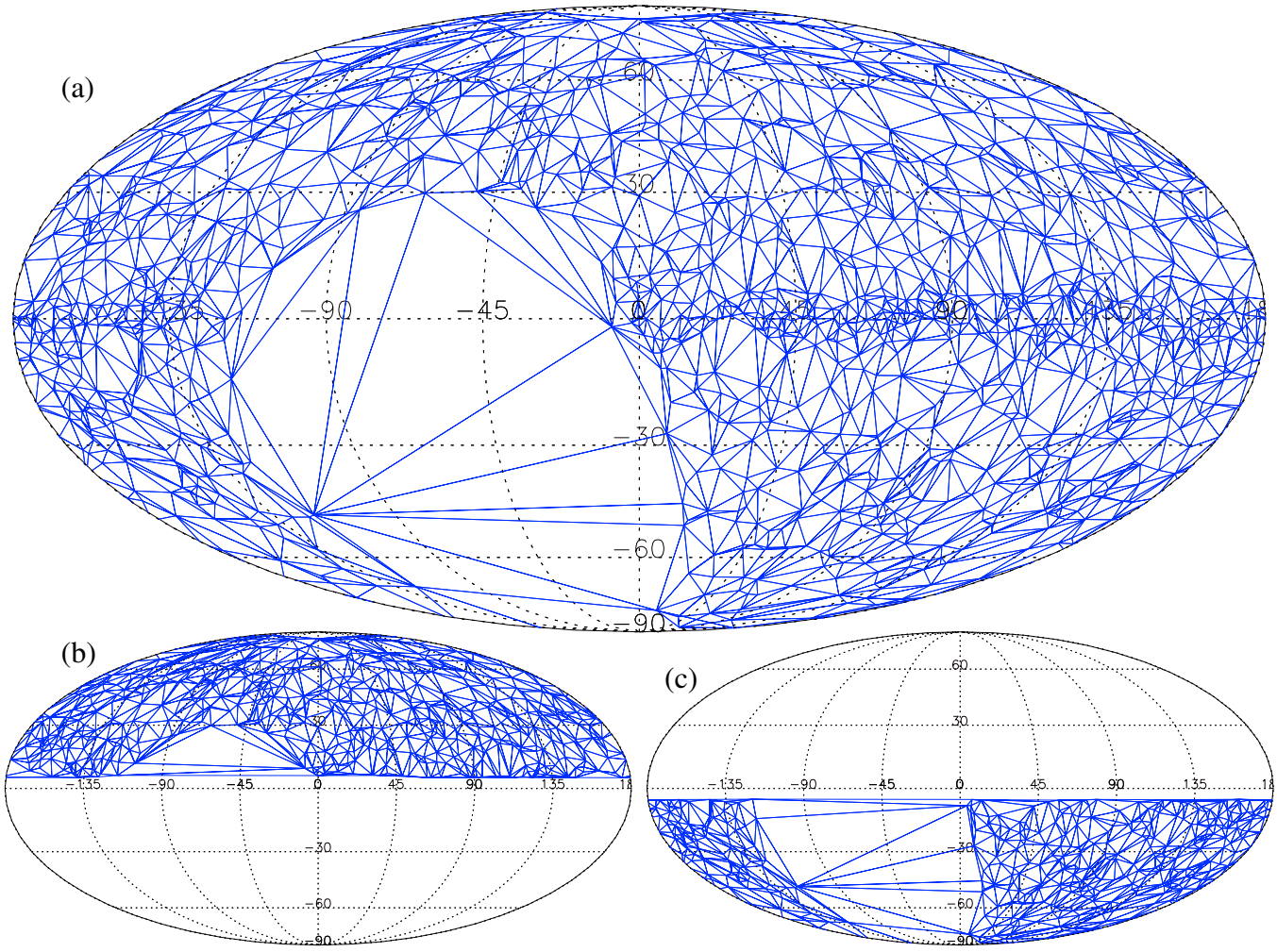

Figure 5. (a) Spatial distribution of 424 (KVNCS2) and 1079 sources (Cal-K, Charlot et al. 2010; Petrov et al. 2011, 2012; Petrov 2012; de Witt et al. 2023) with Delaunay triangles on the galactic plane. (b) Northern region of (a) $b \geq 5°$. (c) Southern region of (a) $b \leq -5°$. (a)–(c) is drawn by the Mollweide equal-area projection technique (abscissa: Galactic longitude (l) [°], ordinate : Galactic latitude (b) [°]).

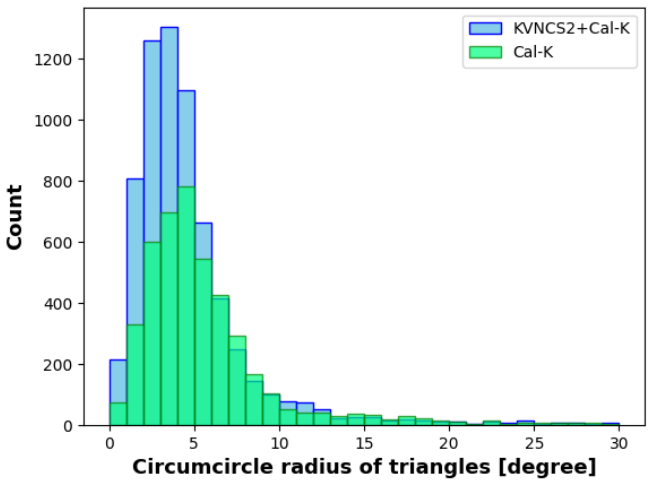

Figure 6. The number distribution of circumcircle radius of Delaunay triangles in $b \leq -5°$ and $5° \geq b$. Skyblue and light green bars present the count from KVNCS2+Cal-K and Cal-K alone, respectively. This figure presents the circumcircle radius of triangles less than 30°.

percentage of missing-flux. On the other hand, there is a difference in the resolution for VLBI data between KVN and KaVA. Their fluxes can come from different regions. The total flux of KaVA can be measured from a more compact region than that of KVN. Nevertheless, the right panel of Figure 7(c) shows a highly linear correlation between KVN and KaVA. The correlation coefficient (R^2) is 0.99 and 0.96 of total-total and total-unresolved fluxes, respectively. This implies that 62 sources in the KVN observation can trace their structure information well and improved the possibility as calibrator candidates from the flux-flux relationship. This suggests the necessity of additional imaging observations to confirm the detailed Fstructural information of new detected sources. KVNCS3 is an ongoing project with KaVA, EAVN, and more extended arrays.

5. Summary

KVNCS2 obtained the VLBI fringes of 424 sources in at least a single-baseline in KVN. Out of 424 sources 347 are new VLBI calibrator candidates in the K band. The spatial distribution of 424 sources is quasi-uniform, while many sources of Cal-K are concentrated on the galactic plane.The calibrators of

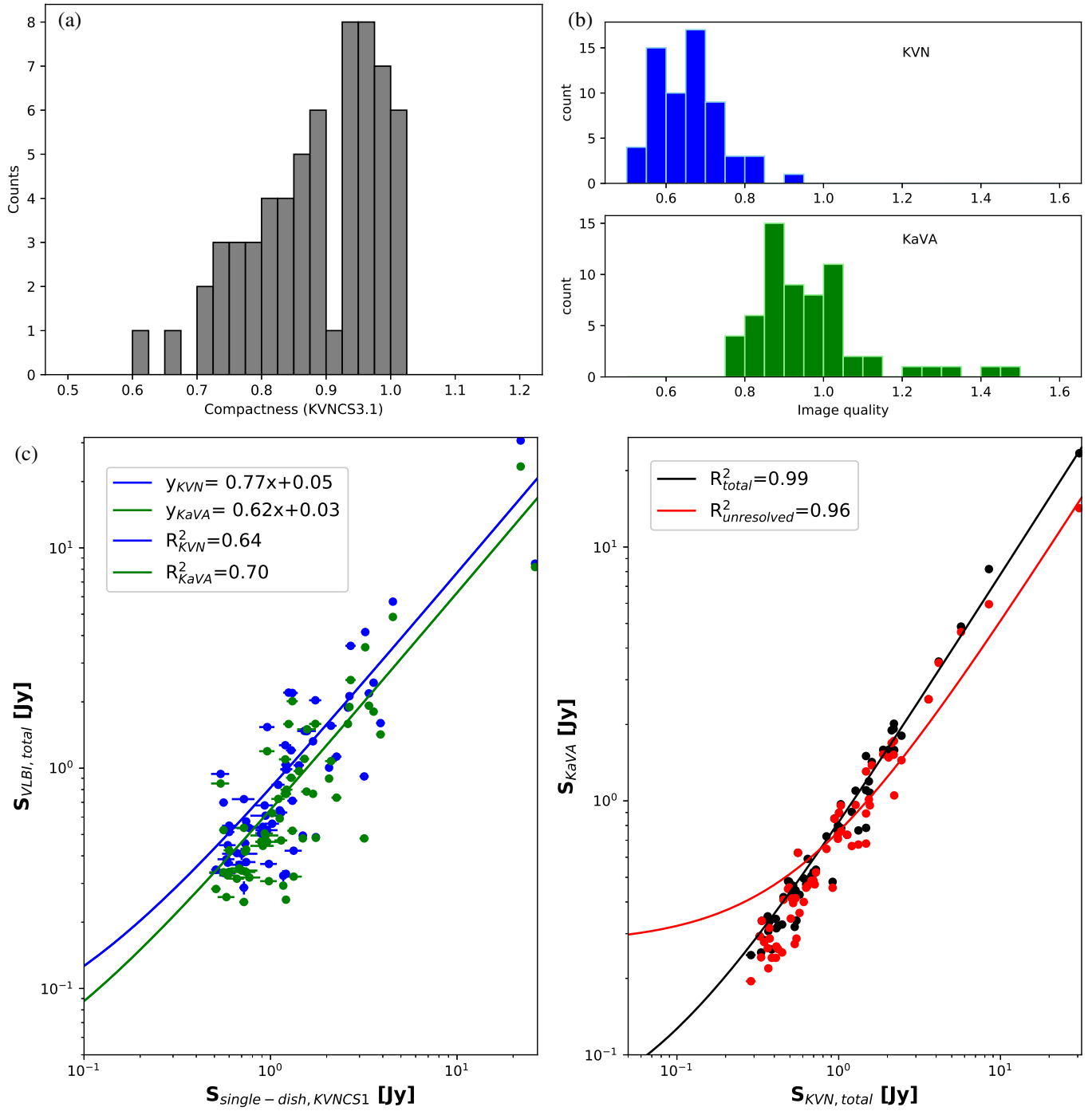

Figure 7. (a) The number distribution of compactness of 62 sources from KVNCS3.1. (b) The number distribution of image quality factor from KVNCS2 (KVN, blue on top) and KVNCS3.1 (KaVA, green on bottom) are presented. (c) Left: The flux-flux relationship between the single-dish from KVNCS1 and the total flux densities from KVN (blue dots) and KaVA (green dots). Blue and green lines present each linear correlation relationship. Right: The relationship of total-total (black dots) and total-unresolved (red dots) flux densities between KVN and KaVA. The black and red lines show each linear correlation. R^2 is the correlation coefficient.

KVNCS2+Cal-K improved the sky coverage by 5% compared to Cal-K alone, assuming a 5° separation angle between the sources. According to the flux-flux relationship of 62 common sources between KVNCS2 and KVNCS3.1 (KVNCS imaging survey with KaVA), the KVNCS2 results of 62 sources trace their structure information. The correlation for these sources improves their possibility as calibrator candidates in the K band. Finally, KVNCS2 can be an additional candidate for a VLBI calibrator at high-frequency and this study suggests the necessity of imaging survey follow-ups with KaVA, EAVN or more extended arrays. The KVN imaging survey (KVNCS3) is an ongoing project (Lee et al., in prep.).

Acknowledgments

We are grateful to the staff of the KVN who helped to operate the array and to correlate the data. The KVN and a high-

performance computing cluster are facilities operated by KASI (Korea Astronomy and Space Science Institute). The KVN observations and correlations are supported through the high-speed network connections among the KVN sites provided by KREONET (Korea Research Environment Open NETwork), which is managed and operated by KISTI (Korea Institute of Science and Technology Information).

Thanks to KaVA (recently EAVN) Science Working Group, which supported the first KVNCS imaging survey (KVNCS3.1) proposal.

References

An, T., Wang, A., Zhang, Y., et al. 2022, MNRAS, 511, 4572
Angioni, R., Ros, E., Kadler, M., et al. 2019, A&A, 627, A148
Beasley, A. J., & Conway, J. E. 1995, in ASPCS, Vol. 82, Very Long Baseline Interferometry and the VLBA, ed. J. A. Zensus, P. J. Diamond, & P. J. Napier, 327
Charlot, P., Boboltz, D. A., Fey, A. L., et al. 2010, AJ, 139, 1713
Charlot, P., Jacobs, C. S., Gordon, D., et al. 2020, A&A, 644, A159
de Witt, A., Jacobs, C. S., Gordon, D., et al. 2023, AJ, 165, 139
Deller, A. T., Brisken, W. F., Phillips, C. J., et al. 2011, PASP, 123, 275
Desai, K. 1998, in AIPS memo 101
Dodson, R., Rioja, M. J., Jung, T.-H., et al. 2014, AJ, 148, 97
Fomalont, E. B., Petrov, L., MacMillan, D. S., Gordon, D., & Ma, C. 2003, AJ, 126, 2562
Gordon, D., Jacobs, C., Beasley, A., et al. 2016, AJ, 151, 154
Han, S.-T., Lee, J.-W., Kang, J., et al. 2008, Int. j. infrared millim. waves, 29, 69
Jung, T. 2018, in 14th European VLBI Netw. Symp. & Users Meet. (EVN 2018), 104
Jung, T., Sohn, B. W., Kobayashi, H., et al. 2011, PASJ, 63, 375
Kovalev, Y. Y., Petrov, L., Fomalont, E. B., & Gordon, D. 2007, AJ, 133, 1236
Krezinger, M., Perger, K., Gabányi, K. É., et al. 2022, ApJS, 260, 49
Lanyi, G. E., Boboltz, D. A., Charlot, P., et al. 2010, AJ, 139, 1695
Lee, J. A. 2017, PhD thesis, Univ. of Sci. and Technol. (UST), Repub. of Korea
Lee, J. A., Sohn, B. W., Jung, T., Byun, D.-Y., & Lee, J. W. 2017, ApJS, 228, 22
Lee, S.-S., Byun, D.-Y., Oh, C. S., et al. 2011, PASP, 123, 1398
Lee, S.-S., Petrov, L., Byun, D.-Y., et al. 2014, AJ, 147, 77
Lee, S.-S., Oh, C. S., Roh, D.-G., et al. 2015, JKAS, 48, 125
Lee, S.-S., Wajima, K., Algaba, J.-C., et al. 2016, ApJS, 227, 8
Lobanov, A. P., Krichbaum, T. P., Witzel, A., & Zensus, J. A. 2006, PASJ, 58, 253
Ma, C., Arias, E. F., Eubanks, T. M., et al. 1998, AJ, 116, 516
Petrov, L. 2012, MNRAS, 419, 1097
Petrov, L., Honma, M., & Shibata, S. M. 2012, AJ, 143, 35
Petrov, L., Kovalev, Y. Y., Fomalont, E., & Gordon, D. 2005, AJ, 129, 1163
Petrov, L., Kovalev, Y. Y., Fomalont, E. B., & Gordon, D. 2006, AJ, 131, 1872
Petrov, L., Kovalev, Y. Y., Fomalont, E. B., & Gordon, D. 2008, AJ, 136, 580
Petrov, L., Kovalev, Y. Y., Fomalont, E. B., & Gordon, D. 2011, AJ, 142, 35
Rioja, M. J., Dodson, R., Jung, T., & Sohn, B. W. 2015, AJ, 150, 202
Traianou, E. T. 2020, PhD thesis, Andreas Eckart Univ. of Cologne, Germany
Zhao, G.-Y., Algaba, J. C., Lee, S. S., et al. 2018, AJ, 155, 26
Zhao, G.-Y., Jung, T., Sohn, B. W., et al. 2019, JKAS, 52, 23